2013 European Control Conference (ECC)
July 17-19, 2013, Zürich, Switzerland.

Moving Horizon for Friction State and Parameter Estimation

Max Boegli, Tinne De Laet, Joris De Schutter, and Jan Swevers

Abstract— **Efficient on-line state and parameter estimation is essential for model-based friction compensation in order to track changes of friction characteristics in time and space. This paper presents a moving horizon estimation (MHE) algorithm for on-line friction state and parameter estimation using a smoothed (analytic) version of the Generalized Maxwell-Slip (GMS) model, a multi-state friction model known to describe all essential friction characteristics in presliding and sliding motion. In contrast to the GMS model, which consists of a switching structure to accommodate for its hybrid nature, the Smoothed GMS (S-GMS) model consists of an analytic set of differential equations well suited for gradient-based state and parameter estimation, as in MHE or in extended Kalman filtering (EKF). Moreover, MHE is known to better handle model nonlinearities, disturbances and constraints than EKF. This paper discusses the implementation of an MHE algorithm for the S-GMS friction model and experimentally compares its performance to an EKF implementation for joint state and parameter estimation.**

I. Introduction

Model-based friction compensation uses a friction model to predict friction force and compensate for it. Accurate friction compensation is obtained provided that the friction model structure includes all major friction characteristics, and accurate estimates of the states and the model parameters are available through state and parameter estimation. Moreover, the need exists to track on-line changes in friction dynamics during normal machine operation.

Most existing identification methods are off-line methods that typically use several sets of tailored input signals, where each set excites certain elements of the friction behavior and hence generates data to estimate a subset of the friction model parameters. Off-line friction identification for the LuGre [1] and Maxwell-slip models using dynamic nonlinear regression is discussed in [2] and [3]. Auto-tuning of feedforward friction compensation based on gradient methods has been used with a simplified LuGre model without Stribeck effect [4]. Friction estimation based on the Elasto-Plastic model [5] has been investigated [6]. The Generalized Maxwell-Slip (GMS) model [7] is known to be able to describe all essential friction characteristics, which is not the case for the above mentioned models. Identification and compensation of friction based on the GMS model are implemented in [8], [9], and [10]. Yet, the switching state conditions between presliding and sliding limit the use of the GMS model in gradient-based optimization techniques for on-line state and parameter estimation, such as in Moving Horizon Estimation (MHE) algorithms [11], [12], or in Extended Kalman Filtering (EKF). To overcome this limitation, a smoothed (analytic) version of the multi-state GMS model, called S-GMS, has been proposed in [13] and [14].

In this work, an MHE algorithm is implemented for friction state and parameter estimation based on the S-GMS model. Experimental results show that the MHE performs similarly to the EKF for state estimation, while offering a smoother parameter estimation. These results confirm previous studies [15], [12], and [16], that MHE is expected to perform similarly or better than EKF for nonlinear dynamical systems.

The paper is organized as follows. First, in section II, the S-GMS friction model is briefly reviewed before emphasizing its main properties. In section III, an MHE algorithm is implemented for state and parameter estimation using the S-GMS friction model. Experimental validation is carried out in section IV, where the MHE is compared to the EKF for joint state and parameter estimation. Finally, in section V, conclusion and future work are presented.

II. Friction Modeling

This section presents the S-GMS friction model, which is used in the MHE implementation. The relation of the S-GMS to the GMS, LuGre and EP friction models is also outlined.

A. The S-GMS Friction Model

The S-GMS model is a multi-state dynamic friction model [13] [14], similar to the GMS model [7], relating the velocity $\dot{q}$ of the object to the friction force y_f depending on an internal state vector $\boldsymbol{z} \in \mathbb{R}^{n_z}$. The S-GMS model consists of a differential state equation $\dot{\boldsymbol{z}} = \boldsymbol{\varphi}(\boldsymbol{z}, \dot{q})$ and a friction force equation $y_f = h(\boldsymbol{z}, \dot{q})$. Each state variable z_i represents the deflection of a spring element i (Fig. 1).

The S-GMS differential state equations are defined as

$$\frac{dz_i}{dt} = \dot{q} - \eta(z_i, \dot{q})\dot{q}_+ \frac{z_i}{z_i^{s_+}(\dot{q})}, \tag{1}$$

and the resulting friction force equation is denoted as

$$y_f = \sum_{i=1}^{n_z} (\kappa_i z_i + \sigma_i \dot{z}_i) + \sigma_v \dot{q}. \tag{2}$$

In (1), $z_i^{s_+}(\dot{q}) = \frac{\nu_i}{\kappa_i} s_+(\dot{q})$ is a positive steady-state deflection corresponding to a normalized fraction ν_i (with $\sum \nu_i = 1$) of the positive velocity weakening

This work benefits from K.U.Leuven-BOF PFV/10/002 Center-of-Excellence Optimization in Engineering (OPTEC), the Belgian Programme on Interuniversity Attraction Poles, initiated by the Belgian Federal Science Policy Office (DYSCO), the European research project EMBOCON FP7-ICT-2009-4 248940, and K.U.Leuven's Concerted Research Action GOA/10/11. Also, the Swiss Company ETEL is gratefully acknowledged for its support. Tinne De Laet is a Postdoctoral Fellow of the Research Foundation - Flanders (FWO-Vlaanderen). All authors are with the Department of Mechanical Engineering, division PMA, K.U.Leuven, 3000 Leuven, Belgium. max.boegli@mech.kuleuven.be

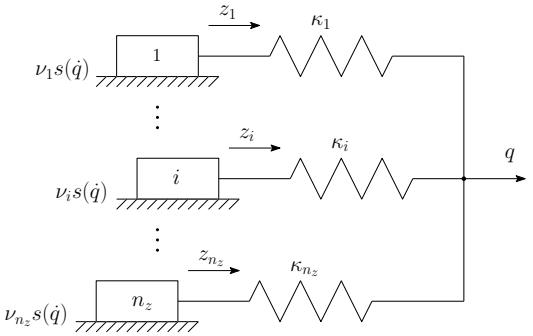

Fig. 1. Representation of the Maxwell-slip friction model using n_z elasto-plastic elements, which all have one common input displacement q. Each of the massless element i has an output force $\kappa_i z_i$, characterized with a stiffness κ_i, a spring deflection z_i (state variable), and a slip (or saturation) force limit $\pm\nu_i s_+(\dot{q})$.

(Stribeck) function $s_+(\dot{q}) = f_C\left(1+\beta e^{-(\dot{q}/v_s)^2}\right)$, with $\beta = \frac{f_S - f_C}{f_C} > -1$ a relation between the static force f_S and the Coulomb force f_C, and v_s the Stribeck velocity. $\dot{q}_+$ represents the absolute value of the velocity $\dot{q}_+ = |\dot{q}|$. The discontinuity at $\dot{q} = 0$ is allowed, as the velocity is not part of the state variables[1]. In both (1) and (2), κ_i is the stiffness of element i. In (2) only, σ_i's are optional micro-viscous friction coefficients and σ_v a macro-viscous friction coefficient.

In (1), $\eta_i(z_i, \dot{q}) \in (0,1)$ is a smoothed transition function between presliding ($\eta_i \simeq 0$) and sliding ($\eta_i \simeq 1$) regime for each element i. η_i consists of two multiplicative terms:

$$\eta_i(z_i,\dot{q}) = \overbrace{\left(1 \mp \tfrac{1}{2}\tanh\left[\lambda\left(\frac{z_i}{z_i^{s+}(\dot{q})} \pm \zeta\right)\right]\right)}^{\eta_{A_i}(z_i,\dot{q})} \times \underbrace{\left(\tfrac{1}{2} + \tfrac{1}{2}\tanh\left(\gamma \frac{z_i}{z_i^{s+}(\dot{q})}\frac{\dot{q}}{v_s}\right)\right)}_{\eta_{B_i}(z_i,\dot{q})} \quad (3)$$

where the transition function η_{A_i}, shown in Fig. 2(a), vanishes when $|z_i| < \zeta z_i^{s+}$ (presliding), and reaches unity otherwise (sliding). The parameter λ sets the transition sharpness of η_{A_i} in (3) while the parameter $\zeta \in [0.7, 1)$ sets the transition points where $\eta_{A_i}(\pm\zeta z_i^{s+}, \cdot) = \frac{1}{2}$. Both parameters ζ and λ are chosen to get η_{A_i} arbitrarily close to one when $|z_i| = z_i^{s+}$, i.e. $\eta_{A_i}(z_i^{s+}, \cdot) = 1 - \alpha$ with $\alpha \in (10^{-2}, 10^{-3})$. Hence, ζ and λ have to satisfy the condition:

$$\tanh(\lambda(1-\zeta)) = 1 - 2\alpha. \quad (4)$$

Fig. 2(a) shows η_{A_i} for three different values of ζ and λ satisfying the condition (4) with $\alpha = 0.01$.

The reset function η_{B_i}, shown in Fig. 2(b), vanishes at velocity reversal (onset of presliding) when $\mathrm{sgn}(\dot{q}) \neq \mathrm{sgn}(z_i)$, while γ sets the transition sharpness. To get a similar slope for η_{B_i} than for η_{A_i}, γ is set equal to λ (Fig. 2(b)).

[1]If the velocity would be part of the state variables, a smoothed approximation of the absolute velocity, e.g. $\dot{q}_+ = \sqrt{\dot{q}^2 + \epsilon}$ with ϵ an arbitrarily small positive constant, could be used.

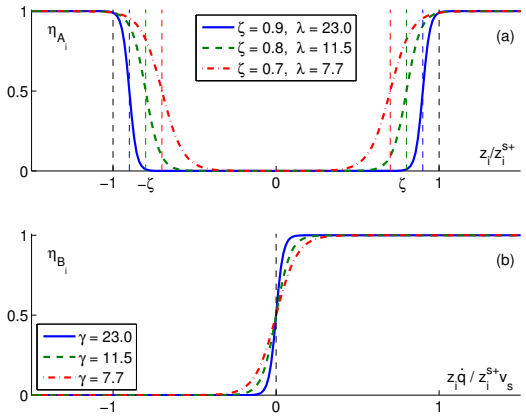

Fig. 2. Smooth sigmoidal-like transition functions η_{A_i} and η_{B_i} between sticking and slipping mode for element i. The element i sticks when $\eta_{A_i}\eta_{B_i} \simeq 0$ and slips when $\eta_{A_i}\eta_{B_i} \simeq 1$. The smoothing function η_{A_i} is shown in (a) for three different values of ζ and λ while satisfying the condition $\eta_{A_i}(1,\cdot) = 0.99$. Correspondingly, the smoothing function η_{B_i} is shown in (b) for three different values of γ.

B. Properties of the S-GMS model

The S-GMS model benefits from all physical friction properties of the GMS model, as demonstrated in [13] and [14]. The main added value of the S-GMS over the GMS is that the S-GMS provides a completely smooth and differentiable set of ODEs, without conditional switching with regard to the state variables and model parameters. This feature makes the S-GMS well suited for on-line gradient-based estimation techniques such as EKF or MHE for both state and parameter estimation in an optimization framework [17].

For the sake of generality, if the number of states in (1) reduces to one ($n_z = 1$) the S-GMS is similar to the single-state Elasto-Plastic (EP) friction model [5], [6]. Additionally, if the smoothing function $\eta = 1$ the S-GMS model boils down to the LuGre model [1]. The state equation (1) is indeed closely related to the single-state Elasto-Plastic (EP) friction model. Hence, the S-GMS model can also be viewed as a multi-state EP model. The EP model uses a piecewise continuous transition function (of class $\mathcal{C}^1$) between the presliding and sliding regime. On the other hand, the S-GMS model introduces an analytic transition function, which is infinitely differentiable (also known as smooth or $\mathcal{C}^\infty$).

A friction model with a multi-state representation such as the S-GMS model allows the presliding hysteresis behavior to be shaped through the elements' stiffnesses distribution (κ_i, ν_i) as shown in Fig. 3, while guarantying the nonlocal memory effect [7]. The ability to shape the hysteresis curvature in presliding is a major advantage of a multi-state model such the S-GMS. Experimental friction state and parameter estimation in Section IV aims to update the stiffness parameters $\boldsymbol{\kappa} \in \mathbb{R}^{n_z}$.

III. The Estimation Framework

This section first presents the general friction force estimation framework. Then, the Moving Horizon Estimator (MHE) for state and parameter estimation is formulated and implemented for the S-GMS friction model.

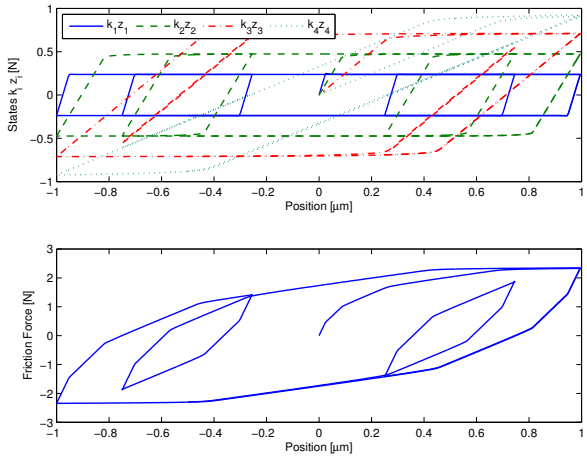

Fig. 3. S-GMS hysteresis behavior with nonlocal memory during presliding. (a) Four internal states z_i multiplied by their respective stiffnesses κ_i. (b) Friction force $y_f = \boldsymbol{\kappa}^T \boldsymbol{z}$. The S-GMS friction parameters are $n_z = 4$ elements, $\boldsymbol{\kappa} = [\ 10,\ 5,\ 2.5,\ 1.25\ ]^T 10^6$N, $\boldsymbol{\nu} = [0.1,\ 0.2,\ 0.3,\ 0.4\ ]^T$, $f_S = 3$N, $f_C = 2$N, and $v_s = 1\mu$m/s. The smoothing parameters of the S-GMS model are $\zeta = 0.9$ and $\lambda = \gamma = 35$ (to get $\alpha = 10^{-3}$).

A. The Friction Observer

A model of a moving mass m with the actual friction force $y_f = \psi(\cdot)$ is represented in Fig. 4. The mass m is driven through a feedback controller K, which outputs an actuation force u. Based on the position q, one can estimate the friction state vector $\boldsymbol{z}$ and parameter vector $\boldsymbol{p}$ by minimizing an error criterion [block $\mathcal{Z}$] between the estimated friction force $\hat{y}_f = h(\hat{\boldsymbol{z}}, \hat{\boldsymbol{p}}, \tilde{\dot{q}})$ [block $\mathcal{F}$] and the indirect friction force measurement based on the control input $\tilde{y}_f = u - m\tilde{\ddot{q}}$ [block $\mathcal{Y}$] assuming a known mass m and estimates of velocity $\tilde{\dot{q}}$ and acceleration $\tilde{\ddot{q}}$ [block $\mathcal{V}$]. To clarify the notation, we mention that estimated variables from the friction observer [blocks $\mathcal{Z}$ & $\mathcal{F}$] (i.e. $\hat{\boldsymbol{z}}$, $\hat{\boldsymbol{p}}$, $\hat{y}_f$) are denoted by the hat $\hat{}$ sign, while kinematic estimates (i.e. $\tilde{\dot{q}}, \tilde{\ddot{q}}, \tilde{y}_f$) are denoted by the tilde $\tilde{}$ sign. The friction observer [blocks $\mathcal{Z}$ & $\mathcal{F}$] implements the friction model as defined in (1-2).

B. Moving Horizon Estimator (MHE) formulation

We consider the dynamical system (1-2) modeled by the ordinary differential equations (ODE's):

$$\dot{\boldsymbol{z}}(t) = \boldsymbol{\varphi}(\boldsymbol{z}(t), \boldsymbol{p}, \dot{q}(t)), \tag{5}$$
$$y_f(t) = h(\boldsymbol{z}(t), \boldsymbol{p}, \dot{q}(t)), \tag{6}$$

with differential states $\boldsymbol{z} \in \mathbb{R}^{n_z}$, parameters $\boldsymbol{p} \in \mathbb{R}^{n_p}$, the velocity input $\dot{q}$ and the friction force output y_f.

To formulate the estimation problem, the continuous time model (5-6) is transformed into a discrete-time model, with the help of numerical integration, to obtain:

$$\boldsymbol{z}_{k+1} = \boldsymbol{f}(\boldsymbol{z}_k, \boldsymbol{p}, \dot{q}_k) + \boldsymbol{w}_{z_k}, \quad \boldsymbol{z}_0 = \boldsymbol{z}(t_0), \tag{7}$$
$$y_{f_k} = h(\boldsymbol{z}_k, \boldsymbol{p}, \dot{q}_k) + v_k. \tag{8}$$

Here, index k denotes the samples taken at times t_k. To account for unknown disturbances on the system states $\boldsymbol{z}_k$, a state noise term $\boldsymbol{w}_k \in \mathbb{R}^{n_z}$ is added. Measurements errors in the output y_{f_k} are expressed by $v_k \in \mathbb{R}$. Both $\boldsymbol{w}_k$ and v_k are assumed to have a zero-mean Gaussian distribution with covariance $\boldsymbol{Q}_k$ and R_k, respectively. For ease of notation only, the velocity input $\dot{q}$ is assumed to be piecewise constant over the time intervals $t \in [t_k, t_{k+1}]$, denoted by $\dot{q}_k$. However, $\dot{q}_k$ denotes a time series of the velocity sampled at an higher rate, which can be used in the integration step (7).

The main feature of MHE [11] is to look into the past to solve an optimization problem over a finite-time horizon. Based on the above model description, the MHE problem is formulated: At current time t_ℓ, we consider a finite-time horizon containing $N+1$ measurements y_{f_k} taken at time $t_k = t_{\ell-N}, ..., t_\ell$. In addition to state trajectory estimation over the horizon, parameter estimation can be included as a constant optimization variable for the considered horizon. The MHE of the system states $\boldsymbol{z}_k$ and model parameters $\boldsymbol{p}$ corresponds to solving the following nonlinear least-squares problem:

$$\min_{\boldsymbol{z}_k, \boldsymbol{p}} \quad \sum_{k=\ell-N}^{\ell-1} \left\| \boldsymbol{f}(\boldsymbol{z}_k, \boldsymbol{p}, \tilde{\dot{q}}_k) - \boldsymbol{z}_{k+1} \right\|^2_{\boldsymbol{Q}_k^{-1}} \tag{9a}$$
$$+ \sum_{k=\ell-N}^{\ell} \left\| h(\boldsymbol{z}_k, \boldsymbol{p}, \tilde{\dot{q}}_k) - \tilde{y}_{f_k} \right\|^2_{R_k^{-1}} \tag{9b}$$
$$+ \left\| \begin{matrix} \boldsymbol{z}_{\ell-N} - \bar{\boldsymbol{z}}_{\ell-N} \\ \boldsymbol{p} - \bar{\boldsymbol{p}} \end{matrix} \right\|^2_{\boldsymbol{P}_\ell^{-1}}. \tag{9c}$$

In a real-time embedded implementation, this constraint optimization problem is solved at each single time instant ℓ. The first term in the objective function (9a) is the weighted squared difference between the estimated state and model prediction, taking into account the model uncertainty $\boldsymbol{Q}_k$. The second term (9b) is the weighted squared difference between the indirect friction force measurement $\tilde{y}_f$ and the estimated friction $\hat{y}_f = h(\cdot)$, taking into account the measurement uncertainty R_k. Finally, the third term (9c), referred to as the arrival cost, summarizes all available information prior to the data horizon in $(\bar{\boldsymbol{z}}_{\ell-N}, \bar{\boldsymbol{p}})$, and is weighted through the covariance matrix P_ℓ.

C. Numerical Implementation Issues

The unconstrained nonlinear least-squares problem (9) can efficiently be solved with the Gauss-Newton method. Solving the optimization problem (9) requires to perform several Gauss-Newton iterations to reach convergence. To reduce the computational burden, only a single iteration is performed at each time instant ℓ. Then, at the next time instant, the oldest measurement is discarded, and a new one is introduced, while the previously estimated states are used as initial values for the next Gauss-Newton iteration. This approach is known as the Real-Time Iteration (RTI) scheme [12], [18].

Defining the MHE optimization variable $\boldsymbol{x} = [\boldsymbol{z}_{\ell-N}^T, ..., \boldsymbol{z}_\ell^T, \boldsymbol{p}^T]^T$, the residual vector $\boldsymbol{F}(\boldsymbol{x})$ of the nonlinear least-squares problem (9), and the Jacobian $\boldsymbol{J}(\boldsymbol{x}) = \frac{\partial \boldsymbol{F}}{\partial \boldsymbol{x}}$ of the residual can be evaluated. The residual

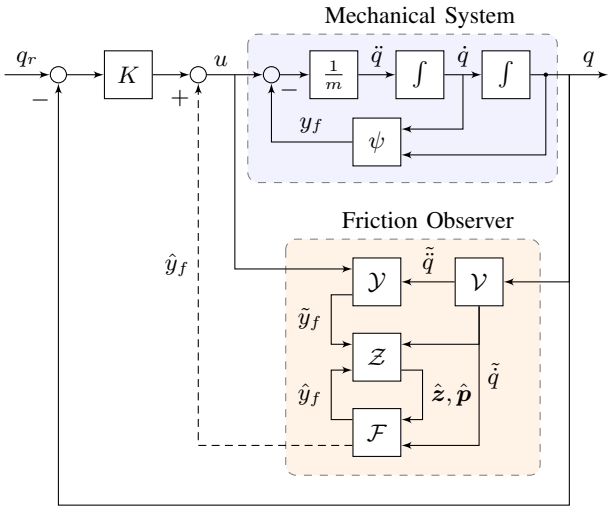

Fig. 4. A moving mass m, subject to friction y_f, is driven by a position feedback controller K to track a reference trajectory q_r. The friction observer comprises four parts: block $\mathcal{V}$, a velocity and acceleration observer; block $\mathcal{Y}$, an indirect friction force measurement $\tilde{y}_f$ based on the control input u minus an inertial term $m\tilde{\ddot{q}}$; block $\mathcal{F}$, the estimated friction $\hat{y}_f$, a function of the estimated states $\hat{\boldsymbol{z}}$, parameters $\hat{\boldsymbol{p}}$, and the velocity input $\tilde{\dot{q}}$; and block $\mathcal{Z}$, a state observer to get the estimated states $\hat{\boldsymbol{z}}$ and parameters $\hat{\boldsymbol{p}}$ from the velocity input $\tilde{\dot{q}}$ and a correction between the indirect friction force measurement $\tilde{y}_f$ and the estimated friction force $\hat{y}_f$. The friction observer [blocks $\mathcal{Z}$ & $\mathcal{F}$] implements the friction model as defined in (7-8).

vector is organized as follows (written at time instant $\ell = N$ to clarify the notation):

$$\boldsymbol{F}(\boldsymbol{x}) = \begin{bmatrix} \boldsymbol{S}_0\ (\boldsymbol{z}_0 - \bar{\boldsymbol{z}}_0) \\ V_0\ (h(\boldsymbol{z}_0, \boldsymbol{p}) - \tilde{y}_{f,0}) \\ \boldsymbol{W}_0\ (\boldsymbol{f}(\boldsymbol{z}_0, \boldsymbol{p}) - \boldsymbol{z}_1) \\ V_1\ (h(\boldsymbol{z}_1, \boldsymbol{p}) - \tilde{y}_{f,1}) \\ \vdots \\ \boldsymbol{W}_{N-1}\ (\boldsymbol{f}(\boldsymbol{z}_{N-1}, \boldsymbol{p}) - \boldsymbol{z}_N) \\ V_N\ (h(\boldsymbol{z}_N, \boldsymbol{p}) - \tilde{y}_{f,N}) \\ \boldsymbol{T}_N\ (\boldsymbol{p} - \bar{\boldsymbol{p}}) \end{bmatrix}, \tag{10}$$

with the weighting matrices $\boldsymbol{S}_0,\ \boldsymbol{T}_0,\ \boldsymbol{W}_k,\ V_k$ related to the inverses of covariance matrices $\boldsymbol{P}_N,\ \boldsymbol{Q}_k,\ R_k$ as follows:

$$\boldsymbol{P}_N^{-1} = \begin{bmatrix} \boldsymbol{S}_0^T \boldsymbol{S}_0 & 0 \\ 0 & \boldsymbol{T}_N^T \boldsymbol{T}_N \end{bmatrix},\ \boldsymbol{Q}_k^{-1} = \boldsymbol{W}_k^T \boldsymbol{W}_k,\ R_k^{-1} = V_k^T V_k. \tag{11}$$

The resulting sparse Jacobian $\boldsymbol{J}(x) = \frac{\partial \boldsymbol{F}}{\partial \boldsymbol{x}}$ is obtained:

$$\begin{bmatrix} \boldsymbol{S}_0 & & & & & 0 \\ V_0\boldsymbol{C}_0 & & & & & V_0\boldsymbol{D}_0 \\ \boldsymbol{W}_0\boldsymbol{A}_0 & -\boldsymbol{W}_0 & & & & \boldsymbol{W}_0\boldsymbol{B}_0 \\ & V_1\boldsymbol{C}_1 & & & & V_1\boldsymbol{D}_1 \\ & \boldsymbol{W}_1\boldsymbol{A}_1 & -\boldsymbol{W}_1 & & & \boldsymbol{W}_1\boldsymbol{B}_1 \\ & & & \ddots & & \vdots \\ & & & & V_N\boldsymbol{C}_N & V_N\boldsymbol{D}_N \\ & & & & & \boldsymbol{T} \end{bmatrix}, \tag{12}$$

with

$$\boldsymbol{A}_k = \left.\frac{\partial \boldsymbol{f}}{\partial \boldsymbol{z}}\right|_{\boldsymbol{z}_k}, \qquad \boldsymbol{B}_k = \left.\frac{\partial \boldsymbol{f}}{\partial \boldsymbol{p}}\right|_{\boldsymbol{z}_k, \boldsymbol{p}}, \tag{13}$$

$$\boldsymbol{C}_k = \left.\frac{\partial h}{\partial \boldsymbol{z}}\right|_{\boldsymbol{z}_k}, \qquad \boldsymbol{D}_k = \left.\frac{\partial h}{\partial \boldsymbol{p}}\right|_{\boldsymbol{z}_k, \boldsymbol{p}}. \tag{14}$$

Sensitivities $\boldsymbol{s_z} = \frac{\partial \boldsymbol{f}}{\partial \boldsymbol{z}}$ and $\boldsymbol{s_p} = \frac{\partial \boldsymbol{f}}{\partial \boldsymbol{p}}$ are either obtained through finite-differences, or better, through the adjoint sensitivity ODE's:

$$\dot{\boldsymbol{s}}_{\boldsymbol{z}} = \frac{\partial \boldsymbol{\varphi}}{\partial \boldsymbol{z}} \boldsymbol{s}_{\boldsymbol{z}} \quad \text{and} \quad \dot{\boldsymbol{s}}_{\boldsymbol{p}} = \frac{\partial \boldsymbol{\varphi}}{\partial \boldsymbol{z}} \boldsymbol{s}_{\boldsymbol{z}} + \frac{\partial \boldsymbol{\varphi}}{\partial \boldsymbol{p}} \tag{15}$$

integrated alongside the model ODE's (5→7). $\frac{\partial \boldsymbol{\varphi}}{\partial \boldsymbol{z}}$ and $\frac{\partial \boldsymbol{\varphi}}{\partial \boldsymbol{p}}$ are the analytic Jacobians of (5) obtained through manual differentiation or automatic differentiation, as implemented in the ACADO Toolkit [17].

1) Set of estimated states and parameters: A common choice for the number of states z_i in the (S)GMS models is $n_z = 4$ [8]. This is a tradeoff between reasonable presliding hysteresis modeling and model complexity. Moreover, we aim to estimate the stiffness parameter vector $\boldsymbol{\kappa} \in \mathbb{R}^{n_z}$ and the Coulomb force f_C, assuming a fixed distribution vector $\boldsymbol{\nu} \in \mathbb{R}^{n_z}$. Thus, the state vector at instant k is $\boldsymbol{z}_k = [\ z_1\ z_2\ z_3\ z_4\ ]_k^T$ and the parameter vector $\boldsymbol{p} = [\ \kappa_1\ \kappa_2\ \kappa_3\ \kappa_4\ f_C\ ]^T$.

2) On the arrival cost: By summarizing past information before $k = \ell - N$, the arrival cost, which can be seen as a regularization term on the initial state $\boldsymbol{z}_{\ell-N}$ and the parameter $\boldsymbol{p}$, ensures stability of the MHE algorithm [19], especially in case of a short horizon or poor observability. Typically, a Riccati recursion is used to update the arrival cost covariance matrix P_ℓ.

3) Benefit of a smoothed model: Evaluation of the Jacobian (12) and sensitivity equations (15) is efficiently carried out from the analytical expression of the S-GMS model (1), which would not have been the case with the switching structure of the GMS. Also, the S-GMS model may benefit from the use of adaptive step-size and implicit ODE solvers.

In the off-line experimental validation (Section IV), the `ode23` solver from MATLAB is used to integrate the S-GMS set of ODE's (1). This Runge-Kutta Bogacki-Shampine scheme is also able to handle the moderate ODE stiffness for higher $\boldsymbol{\kappa}$ values[2]. The MATLAB `lsqnonlin` function using the Levenberg-Marquardt algorithm is used to solve one Gauss-Newton iteration at each time instant ℓ, while providing the function with the user-defined Jacobian $\boldsymbol{J}(\boldsymbol{x})$ (12).

IV. Friction State and Parameter Estimation based on Experimental Data

This section discusses the experimental validation of the MHE for the S-GMS friction model in presliding regime. The results obtained from the MHE are compared to those from an EKF for joint state and parameter estimation.

A. Data Acquisition and Trajectory Profile

Friction state and parameter estimation is validated with experimental input-output data from an XY positioning table (Fig. 5) used in optical wafer inspection. Only one axis (the lower axis) is considered in the experiments. Position q and control input u are sampled at 10kHz. The estimated velocity

[2]In friction model equations, numerical stiffness is closely related to mechanical stiffness.

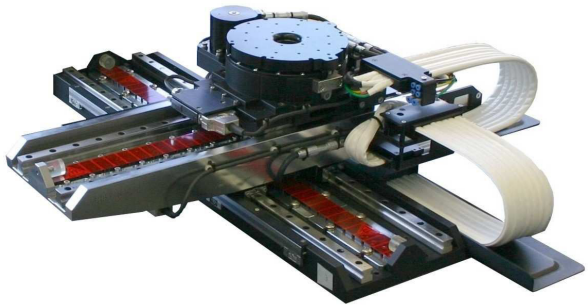

Fig. 5. Direct-drive XY positioning table for wafer inspection

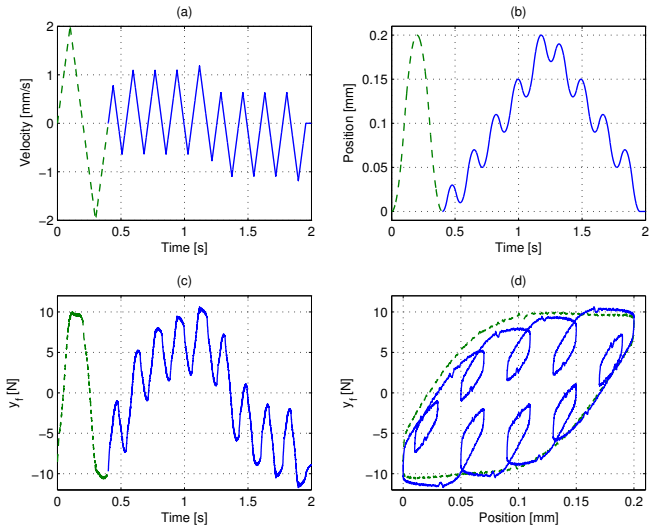

Fig. 6. Experimental trajectory. (a) Measured velocity $\tilde{\dot{q}}$, (b) Measured position q, (c) Indirect friction force measurement $\tilde{y}_f = u - m\tilde{\ddot{q}}$, (d) Friction force vs position depicting minor loops hysteresis.

$\tilde{\dot{q}}$ and acceleration $\tilde{\ddot{q}}$ are obtained by taking the first order finite-difference derivative of the measured position q and the estimated velocity $\tilde{\dot{q}}$, respectively, combined with a second order low-pass filter with a cutoff frequency at 500Hz. The estimated velocity $\tilde{\dot{q}}$ sampled at 10kHz is used in the integration step (7). The indirect friction force measurement $\tilde{y}_f = u - m\tilde{\ddot{q}}$ is sub-sampled at the MHE optimization rate of 100Hz.

The reference trajectory is a back and forth motion with a maximum range of 200μm, combined with smaller motions (minor loops) as shown in Fig. 6(b) for a piecewise linear velocity profile (Fig. 6(a)) and an acceleration of $\pm$0.02m/s^2. The indirect friction force measurement $\tilde{y}_f$ is shown in Fig. 6(c). Fig. 6(d) shows $\tilde{y}_f$ versus the measured position q. Typical minor loops of friction hysteresis are visible.

B. Estimation Setup and Experimental Results

The nominal set of friction parameters used in the MHE and EKF estimators is listed in Table I. These parameters were identified using the virgin curve technique from [8]. The estimated state vector and parameter vector are respectively $\boldsymbol{z} = [\ z_1\ z_2\ z_3\ z_4\ ]^T$ and $\boldsymbol{p} = [\ \kappa_1\ \kappa_2\ \kappa_3\ \kappa_4\ ]^T$. A parameter normalization is introduced for better numerical conditioning. The normalized parameter vector $\boldsymbol{p}'$, without units [-], is defined as $\boldsymbol{p}' = \mathrm{diag}(\boldsymbol{p}_0)^{-1}\boldsymbol{p}$, where $\boldsymbol{p}_0$ is the initial parameter vector $\boldsymbol{\kappa}$ shown in Table I. An horizon length of $N = 20$ samples is chosen for the MHE.

TABLE I

NOMINAL S-GMS FRICTION PARAMETERS VALUES USED FOR THE MHE STATE AND PARAMETER ESTIMATION

S-GMS Parameters	S-GMS Values	Unit
n_z	4	-
$[\ \kappa,\ \nu,\ \sigma\ ]$	$\begin{bmatrix} 120 & 0.067 & 0 \\ 25 & 0.056 & 0 \\ 7.1 & 0.047 & 0 \\ 7.9 & 0.83 & 0 \end{bmatrix}$	[kN/m, -, Ns/m]
σ_v	20	Ns/m
f_C	4	N
β	0.12	-
v_s	10^{-3}	m/s
ζ	0.9	-
$\lambda,\ \gamma$	35 $(\alpha = 10^{-3})$	-

Noise covariance matrices have been set identically between the MHE and EKF. The parameter covariance matrix $\boldsymbol{Q}_p = \sigma_p^2 \boldsymbol{I}_{n_p \times n_p}$ is set with $\sigma_p = 0.05$, i.e. corresponding to 5% of the normalized nominal value. The state noise covariance matrix $\boldsymbol{Q}_z = \mathrm{diag}(\sigma_{z_1}^2, ..., \sigma_{z_{n_z}}^2)$ is set with $\sigma_{z_i} = 0.1\nu_i f_C$, to account for the distribution $\boldsymbol{\nu}$ of the steady-state $\kappa_i z_i^{s+}(\dot{q}) = \nu_i s_+(\dot{q}) \simeq \nu_i f_C$. By analyzing the measurement noise and the uncertainty of the indirect friction force measurement $\tilde{y}_f$, the variance $R = \sigma_y^2$ is set with $\sigma_y = 0.5$N.

Fig. 7 shows the estimated friction $\hat{y}_f$ during the complete trajectory with the MHE and EKF, respectively. It can be noticed that the MHE friction estimate shows a similar behavior than the EKF friction estimate. Fig. 8 shows the estimated parameter $\boldsymbol{p}$ during the complete trajectory with the MHE and EKF, respectively. It can be observed that the MHE parameter estimation shows a smoother convergence behavior than the EKF parameter estimation. The $\pm 2\sigma$ uncertainty bounds are shown in Fig. 8. A linear approximation of the parameter estimation uncertainty for the MHE is given by the Fisher information matrix.

V. CONCLUSION AND FUTURE WORK

This paper presented a MHE algorithm implementation based on the S-GMS friction model for state and parameter estimation. The newly developed S-GMS model consists of a set of analytic ODE's well suited for gradient-based optimization techniques such as in MHE. In this work, algorithm complexity is reduced by casting the MHE into an unconstrained nonlinear least-squares problem and solving only one Gauss-Newton iteration at each time step.

Experimental results of friction state and parameter estimation have been presented and compared between an MHE and EKF implementation. The resulting friction state estimation shows a similar behavior for both the MHE and EKF, while MHE parameter estimation shows a smoother behavior than for the EKF.

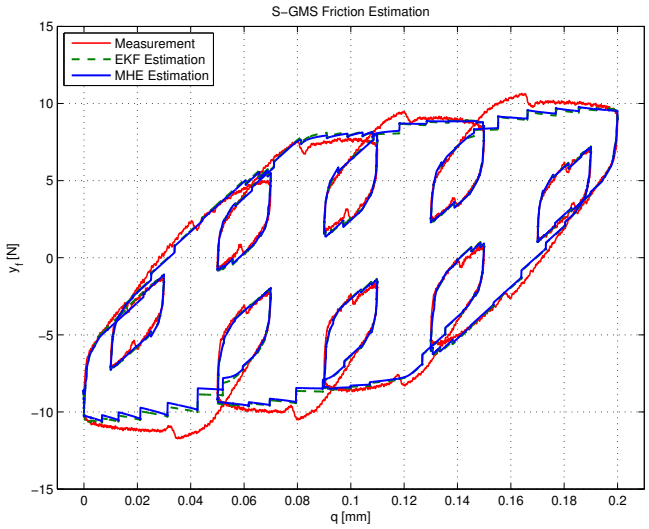

Fig. 7. S-GMS friction force $\hat{y}_f$ estimation.

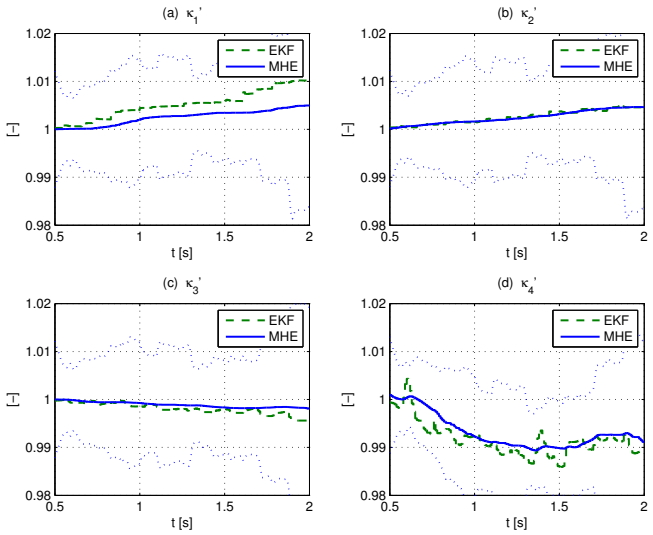

Fig. 8. Normalized S-GMS parameter $\boldsymbol{\kappa}'$ estimation. Uncertainty bounds at $\pm 2\sigma$ are shown.

A real-time version of the MHE algorithm for state and parameter estimation based on the S-GMS friction model is currently developed with ACADO [17], a toolkit for automatic code generation and dynamic optimization, to be implemented on the ETEL XY positioning table to estimate and compensate for friction in real-time. Computation time within a few milliseconds is expected [20].

Acknowledgment

This work benefits from KU Leuven BOF PFV/10/002 Center-of-Excellence Optimization in Engineering (OPTEC), the Belgian Programme on Interuniversity Attraction Poles, initiated by the Belgian Federal Science Policy Office (DYSCO), the European research project EMBOCON FP7-ICT-2009-4 248940, and KU Leuven's Concerted Research Action GOA/10/11. Tinne De Laet is a Postdoctoral Fellow of the Research Foundation - Flanders (FWO-Vlaanderen). The Swiss Company ETEL is gratefully acknowledged for its support.

References

[1] C. Canudas de Wit, H. Olsson, K. Astrom, and P. Lischinsky, "A New Model for Control of Systems with Friction," *IEEE Trans. on Automatic Control*, vol. 40, no. 3, pp. 419–425, 1995.

[2] D. Rizos and S. Fassois, "Friction Identification Based upon the LuGre and Maxwell Slip Models," *IEEE Trans. on Control Systems Technology*, vol. 17, no. 1, pp. 153–160, 2009.

[3] A. Amthor, T. Hausotte, P. Li, C. Ament, and G. Jaeger, "Friction Identification and Compensation on Nanometer Scale," in *Proc. IFAC World Congress*, Seoul, South Korea, 2008.

[4] F. Altpeter, M. Grunenberg, P. Myszkorowski, and R. Longchamp, "Auto-Tuning of Feedforward Friction Based on the Gradient Method," in *Proc. American Control Conference*, Chicago, Illinois, 2000.

[5] P. Dupont, V. Hayward, B. Armstrong, and F. Altpeter, "Single State Elastoplastic Friction Models," *IEEE Trans. on Automatic Control*, vol. 47, no. 5, pp. 787–792, 2002.

[6] V. Hayward, B. Armstrong, F. Altpeter, and P. Dupont, "Discrete-Time Elasto-Plastic Friction Estimation," *IEEE Trans. on Control Systems Technology*, vol. 17, no. 3, pp. 688–696, 2009.

[7] F. Al-Bender, V. Lampaert, and J. Swevers, "The Generalized Maxwell-Slip Model: A Novel Model for Friction Simulation and Compensation," *IEEE Trans. on Automatic Control*, vol. 50, no. 11, pp. 1883–1887, 2005.

[8] Z. Jamaludin, H. Van Brussel, and J. Swevers, "Quadrant Glitch Compensation using Friction Model-Based Feedforward and an Inverse-Model-Based Disturbance Observer," in *Proc. IEEE Intl Workshop on Advanced Motion Control*, 2008.

[9] C. Casanova, E. De Pieri, U. Moreno, and E. Castelan, "Friction Compensation in Flexible Joints Robot with GMS Model: Identification, Control and Experimental Results," in *Proc. IFAC World Congress*, Seoul, South Korea, 2008.

[10] I. Nilkhamhang and A. Sano, "Model-based Adaptive Friction Compensation for Accurate Position Control," in *Proc. IEEE Conf. on Decision & Control*, 2008.

[11] D. Robertson, J. Lee, and J. Rawlings, "A Moving Horizon-Based Approach for Least-Squares Estimation," *AIChE Journal*, vol. 42, no. 8, pp. 2209–2224, 1996.

[12] P. Kuehl, M. Diehl, T. Kraus, J. Schloeder, and H. G. Bock, "A Real-Time Algorithm for Moving Horizon State and Parameter Estimation," *Computers and Chemical Engineering*, vol. 35, pp. 71–83, 2011.

[13] M. Boegli, T. De Laet, J. De Schutter, and J. Swevers, "A Smoothed GMS Friction Model for Moving Horizon Friction State and Parameter Estimation," in *Proc. IEEE Intl Workshop on Advanced Motion Control*, Sarajevo, Bosnia and Herzegovina, 2012.

[14] ——, "A Smoothed GMS Friction Model suited for Gradient-Based Friction State Estimation," in *Proc. American Control Conference*, Montreal, Canada, 2012.

[15] E. Haseltine and J. Rawlings, "Critical Evaluation of Extended Kalman Filtering and Moving Horizon Estimation," *Ind. Eng. Chem. Res.*, vol. 44, no. 2, pp. 2451–2460, 2005.

[16] T. Poloni, A. Eielsen, B. Rohal-Ilkiv, and T. Johansen, "Moving Horizon Observer for Vibration Dynamics with Plant Uncertainties in Nanopositioning System Estimation," in *Proc. American Control Conference*, Montreal, Canada, 2012.

[17] B. Houska, H. Ferreau, and M. Diehl, "ACADO Toolkit - An Open-Source Framework for Automatic Control and Dynamic Optimization," *Optimal Control Applications and Methods*, vol. 32, no. 3, pp. 298–312, 2011, http://acadotoolkit.org.

[18] M. Diehl, H. Bock, J. Schloeder, R. Findeisen, Z. Nagy, and F. Allgoewer, "Real-Time Optimization and Nonlinear Model Predictive Control of Processes governed by Differential-Algebraic Equations," *Journal of Process Control*, vol. 12, pp. 577–585, 2002.

[19] C. Rao, J. Rawlings, and D. Mayne, "Constrained State Estimation for Nonlinear Discrete-Time Systems: Stability and Moving Horizon Approximations," *IEEE Trans. on Automatic Control*, vol. 48, no. 2, pp. 246–258, 2003.

[20] H. Ferreau, T. Kraus, M. Vukov, W. Saeys, and M. Diehl, "High-Speed Moving Horizon Estimation based on Automatic Code Generation," in *Proc. IEEE Conference on Decision and Control*, Maui, Hawaii, 2012.